P. aeruginosa **disrupts CDC-42/ARP-2/3 mediated F-actin organization to induce intestinal deformation in** ***C. elegans***

Authors: AN Divyashree, Tanushree Sinha and Anup Padmanabhan[1]*

Affiliations:

[1]Department of Biology, Trivedi School of Biosciences, Ashoka University, Sonipat, Haryana India -131029

*Correspondence to: anup.padmanabhan@ashoka.edu.in

ORCiD ids:

0000-0003-3127-2132 (AN Divyashree)

0009-0000-7405-283X (Tanushree Sinha)

0000-0001-6007-6929 (Anup Padmanabhan)

SUMMARY

Apico-basal polarity maintains the integrity of cortical actin cytoskeleton and regulates secretory functions in intestinal epithelium essential for barrier defense against infections. The opportunistic pathogen, *Pseudomonas aeruginosa*, exploits the interplay between cell polarity and cytoskeletal machineries to subvert these defenses. Mechanistic insights into such pathogen-induced cytoskeletal alterations have largely been derived from *in-vitro* epithelial monolayers, which may not capture the influences of multicellular physiology such as tissue mechanics, and innate immunity. Here, we show that the extracellular *P. aeruginosa* disrupts apical polarity in *C. elegans* enterocytes, leading to fragmentation of ARP-2/3 clusters and disorganization of apical F-actin. This disruption causes shedding of actin-rich vesicles into lumen and a pronounced apical deformation. Inhibition of CDC-42-mediated actin polymerization or PI3K-AKT signalling attenuated enterocyte deformation and extended the lifespan of *C. elegans* upon *P. aeruginosa* exposure. Our findings reveal a conserved strategy by which *P. aeruginosa* exploits cellular polarity machinery to disrupt host actin organization during extracellular infection of the intestinal epithelium.

Keywords : F-actin / ARP-2/3 / CDC-42 / Polarity / *P. aeruginosa*/ Host-pathogen

INTRODUCTION

Symbiotic interactions with the gut microbiota are essential for maintaining health and metabolism in metazoans. Constantly exposed to a diverse micro-organisms, the intestinal epithelium acts as a frontline sentinel for immune surveillance, detecting perturbations caused by dysbiosis, distinguishing harmless commensals from pathogens, and mounting context-appropriate immune response. During infection, bacterial pathogens elicit a wide range of responses from intestinal epithelial cells - some orchestrated by the pathogens to promote their survival and dissemination, and others initiated by the host to limit damage and trigger innate immunity. Unlike professional immune cells, enterocytes lack canonical pathogen recognition receptors (PRRs) that detect microbe-associated molecular patterns (MAMPs). Instead, they respond to pathogen effector activity and the disruptions they cause to physiological processes and cellular homeostasis, collectively termed “patterns of pathogenesis”. These include damage associated molecular patterns (DAMPs) triggered by pathogen effectors. Studies in model organisms such as *Drosophila melanogaster* and *Caenorhabditis elegans (C. elegans)* have highlighted the role of effector-triggered, cell autonomous surveillance in epithelial immunity (Stuart *et al*, 2013; Tse-Kang *et al*, 2025; Vance *et al*, 2009).

C. elegans, a bacterivorous soil nematode, inhabits microbe-rich environments and encounters a broad spectrum of microorganisms, including pathogens (Berg *et al*, 2016; Schulenburg & Félix, 2017). While a protective cuticle (Gravato-Nobre *et al*, 2005) and sophisticated pathogen-avoidance behaviours (Lei *et al*, 2024; Melo & Ruvkun, 2012; Pereira *et al*, 2020; Prakash *et al*, 2021; Singh & Aballay, 2019b; Zhang *et al*, 2005) limit exposure, the intestinal epithelium remains the primary site of infection due to the worm’s bacterial diet. Ingested bacteria are mechanically ground in the pharynx before entering the lumen, yet some pathogens survive, proliferate, and colonize the intestine. The *C. elegans* intestine is composed of 20 polarized epithelial cells arranged longitudinally, with apical surfaces facing the central lumen and basolateral surface engaged in cell-cell and cell-matrix adhesions (Dimov & Maduro, 2019; McGhee, 2007). The apical surface is enriched in microvilli, providing the primary site for host-pathogen interaction (MacQueen *et al*, 2005a) (Fig. 1B). Polarity is maintained by structural and signalling complexes: the Crumbs complex (CRB-1,

CRB-3, MAGUK-2) and the PAR complex (comprising PAR-3, PAR-6, PKC-3 kinase and CDC-42 GTPase) localize apically, while the Scribble complex (LET-413, LGL-1, and DLG-1) and PAR-1 kinase localize basolaterally. Lipids are also polarized, with phosphatidylinositol 4,5-bisphosphate [PI(4,5)P_2 or PIP_2] enriched apically and phosphatidylinositol 3,4,5-trisphosphate [PI(3,4,5)P_3 or PIP_3] basolaterally. This polarity is reinforced by polarity complexes, cytoskeletal organization, membrane trafficking, and junctional assemblies. (Armenti & Nance, 2012; Bossinger *et al*, 2004; Legouis *et al*, 2000; Winter *et al*, 2012). Membrane polarity is also essential for the spatial localization and activation of Rho family GTPases (Jaffe & Hall, 2005). In particular, CDC-42 activates the ARP-2/3 complex to promote branched actin polymerization, essential for the assembly and maintenance of apical microvilli (Bernadskaya *et al*, 2011; Ma *et al*, 1998; Martin-Belmonte *et al*, 2007; Shafaq-Zadah *et al*, 2012; Thuenauer *et al*, 2022). During infection many pathogens employ diverse virulence strategies to subvert the host polarity and actin cytoskeletal machinery to alter cellular shape and mechanics (Ruch & Engel, 2017). This facilitates intracellular entry and spread, or extracellular effector-induced inflammation and tissue damage (Bastounis *et al*, 2022; Colonne *et al*, 2016). Conversely, epithelial cells may actively reorganize actin as part of their defense response. Thus, plasma membrane polarity-actin cytoskeleton cross talk is vital for epithelial integrity during infection (Fleiszig *et al*, 1997; Tran *et al*, 2014).

The opportunistic pathogen, *Pseudomonas aeruginosa* a major cause of nosocomial infections and infects a wide range of hosts, including *C. elegans* (Balla & Troemel, 2013; Mahajan-Miklos *et al*, 1999; Tan *et al*, 1999a). In worms, *P. aeruginosa* infection induces diverse stress responses, mitotic quiescence, and apoptosis (Kuss-Duerkop & Keestra-Gounder, 2020; Pellegrino *et al*, 2014; Dunbar *et al*, 2012; McEwan *et al*, 2012; Bollen *et al*, 2024). In the absence of professional immune cells, *C. elegans* upon detecting infection activate innate immune signalling such as the TIR-1-p38 MAP kinase and the DAF-2/DAF-16 insulin/IGF-1 pathways (Peterson *et al*, 2023). DAF-2 dependent phosphorylation of PI3K/AGE-1 recruits AKT-1/AKT-2 kinases that in turn phosphorylate DAF-16. This kinase cascade results in cytoplasmic retention of DAF-16, thereby regulating gene expression (Ewbank, 2006). DAF-16 is known to induce expression of antimicrobial genes, detoxifying enzymes and bacterial avoidance (Balla

& Troemel, 2013; Cohen & Troemel, 2015; Irazoqui *et al*, 2010; Peterson *et al*, 2022; Pukkila-Worley & Ausubel, 2012). Avoidance behaviour is also triggered by mechanical cues, such as intestinal distension ("bloating"), mediated by TRPM channels (Filipowicz *et al*, 2021; Kumar *et al*, 2019; Singh & Aballay, 2019b, 2019a). Here, we investigated the mechanism underlying cytoskeletal remodelling and polarity disruption following *P. aeruginosa* infection. We find that *P. aeruginosa* exploits PI3K-AKT pathway to perturb CDC-42-ARP-2/3-mediated actin organization in C. elegans enterocytes. The resultant disruption in epithelial polarity and loss of actin rich vesicles from the apical surface locally alters the surface mechanics resulting in deforms intestinal lumen surface contributing to host lethality.

RESULTS

Pseudomonas aeruginosa **infection results in** ***C. elegans*** **intestinal deformation**

Consistent with previous studies, exposure to *P. aeruginosa* strain PA14 resulted in reduced *C. elegans* survival (lifespan^{PA14} ~8 days; TD_{50}^{PA14} ~3 days) compared to *E. coli* (OP50) (lifespan^{OP50} ~18 days; TD_{50}^{OP50} ~8 days) (Fig 1A). This lethality has been partly attributed to the colonization of the intestinal lumen by *P. aeruginosa* (Tan *et al*, 1999a). To examine the impact *P. aeruginosa* infection on host cytoskeletal organization, we imaged *C. elegans* intestines expressing mCherry fused to the N-terminus of ACT-5, the intestine specific actin isoform (MacQueen *et al*, 2005b; Szumowski *et al*, 2016). In *E. coli* fed worms, ACT-5, appeared as smooth parallel lining along the intestinal lumen (Fig. 1B and 1C; blue arrowhead, OP50). Despite age related intestinal distension (Egge *et al*, 2019; Irazoqui *et al*, 2010; Singh & Aballay, 2019a) the ACT-5 signal remained smooth even after 3 days on OP50 (Fig.1C; red double-headed arrows in OP50/day-3, and S1A). Although lumen was distended following *P. aeruginosa* exposure (Fig. 1C, red double-headed arrows in PA14 day-3, and Fig S1A), apical surface characteristics were markedly distinct. In contrast to the smooth surface seen in *E. coli*-fed animals, *P. aeruginosa*-fed worms displayed extensive wrinkles and surface deformations (Fig. 1C; PA14,filled red arrowheads), with vesicle-like structures budding outward from the deformed apical surface (Fig. 1C; PA14, red arrows in enlarged ROI). Whereas only ~4% (2/54) of *E. coli*-fed worms

140 showed such deformations after 1-day, ~48%(27/56) of *P. aeruginosa* -exposed
141 worms did (Fig. 1C). By day-3, the incidence rose to ~83% (43/52) in *P. aeruginosa*-
142 fed worms compared to ~19% (10/52) on *E. coli*.

143

144 **Magnitude of intestinal deformation depends on the duration *of P. aeruginosa***
145 **infection**

146 To quantify changes in intestinal morphology, we defined a dimensionless "apical
147 deformation index" (δ_{apical}), as the ratio of apical lumen length to total worm length (Fig.
148 1E). *E. coli*-fed worms consistently maintained 'δ_{apical}^{OP50}=1', whereas P. aeruginosa
149 exposure resulted in 'δ_{apical}^{PA14}>1', with values increasing over time, indicating
150 progressive deformation (Fig. 1F). Tracking individual worms revealed that worms fed
151 with *E. coli* , the value of δ_{apical}^{OP50}~1, but in worms exposed to *P. aeruginosa*
152 deformation was evident by day 1 and worsened over subsequent days (Fig. 1G). In
153 acute infection assays, 12-hour exposure did not cause significant deformation,
154 whereas 24-hour exposure induced noticeable apical distortion even after transfer
155 back to *E.coli* (Fig. S1B). To test whether deformation extended beyond the apical
156 surface, we examined transgenic worms co-expressing LET-413::mCherry and DLG-
157 1::GFP, the Scribble and Discs Large orthologs in *C. elegans,* as markers for
158 basolateral surface and AJ, respectively (Fig. 5A) (Bossinger *et al*, 2004; Legouis *et*
159 *al*, 2000; McMahon *et al*, 2001; Riga *et al*, 2021). Neither AJ positioning nor basal
160 deformation index (δ_{basal}) was significantly altered by *P. aeruginosa* exposure (Fig. 5A
161 and S1C). However, lateral surfaces showed LET-413 enrichment and altered
162 morphology (Fig. 5A and 5C), indicating that deformation was restricted to apical and
163 lateral domains. Next we confirmed that the intestinal deformation was independent of
164 germline or uterine expansion by examining males, which lack these tissues (Fig. S1D
165 and S1E). F-actin staining using Phalloidin-AlexaFluor647 and LifeAct::mRuby
166 expression showed visible apical deformation specifically upon *P. aeruginosa*
167 exposure, eliminating the possibility that the infection phenotype might be an artifact
168 of mCherry::ACT-5 transgene expression. (Fig. S1F and S1H, red filled arrowheads).
169 Finally, we validated the phenotype using additional apical/sub-apical markers: PGP-
170 1::GFP, ERM-1::GFP, PAR-6::GFP, and IFB-2::GFP, that localized to apical

171 membrane, microvillar structure or subapical positions, respectively (Fig. 1H) (Geisler
172 *et al*, 2020; Göbel *et al*, 2004; Sepers *et al*, 2022). In all cases, *P. aeruginosa* exposure
173 resulted in clear deformation of the apical surface topology. 'Slow killing' assay,
174 typically uses nematode growth media (NGM) containing 0.35% peptone(Tan *et al*,
175 1999a). To minimize any confounding effects from elevated peptone concentrations
176 on intestinal epithelial response, we conducted our infections on standard NGM
177 containing 0.25% peptone, optimised for *C. elegans* growth (Stiernagle, 2006). We
178 observed intestinal deformation in worms infected on 0.35% peptone media
179 indistinguishable from 0.25% peptone (Fig. S1I and S1J). Our lifespan assays mirrored
180 previously reported kinetics using 0.35% peptone-containing NGM (Figure 1A) (Tan
181 *et al*, 1999a). Thus we confirmed that our infection conditions faithfully recapitulate
182 chronic *P. aeruginosa* infection, leading to progressive apical and lateral intestinal
183 deformation.

184

185 **CDC-42 mediates *Pseudomonas*-induced intestinal deformation**

186 RHO family GTPases are the key upstream regulators of F-actin assembly and
187 organization, that co-ordinate actin dynamics in a spatiotemporally controlled manner
188 (Ann Mack & Georgiou, 2014; Jaffe & Hall, 2005). *P. aeruginosa* infecting MDCK cells
189 disrupt RHO signalling through effector proteins that interfere with GTPase-activating
190 proteins (GAPs), leading to the disorganization of actin architecture (Cowell *et al*,
191 2005; Kazmierczak & Engel, 2002; Krall *et al*, 2000; Pederson *et al*, 1999; Sun &
192 Barbieri, 2004). To test whether *Pseudomonas* induced surface deformation in *C.*
193 *elegans* enterocytes might similarly depend on RHO GTPase-mediated actin re-
194 organization, we individually depleted RHO-1, CED-10, and CDC-42 in adult worms
195 expressing intestinal mCherry::ACT-5, and subsequently exposed them to *P.*
196 *aeruginosa* or *E. coli*. As in controls, exposure to *P. aeruginosa* resulted in apical
197 deformation in *rho-1(RNAi)* or *ced-10(RNAi)* animals (Fig. 2A, S2A and S2B). In
198 contrast, *cdc-42(RNAi)* worms exposed to *P. aeruginosa* displayed no deformation
199 (Fig. 2A and 2B). This lack of deformation was not due to impaired pathogen sensing
200 in *cdc-42(RNAi)* worms (Fig. S2D and S2E) (Estes *et al*, 2010). Consistent with its role
201 in supressing intestinal deformation, *cdc-42(RNAi)* worms exhibited significantly

extended total lifespan (8 days) compared to RNAi controls (4 days) upon *P. aeruginosa* exposure (Fig. 2C).

P. aeruginosa **infection leads to cytoplasmic accumulation of G-actin**

The absence of intestinal deformation in *cdc-42(RNAi)* worms prompted us to investigate the intracellular localization of CDC-42 and its downstream effector, the actin nucleating ARP-2/3 complex, during *P. aeruginosa* infection. We used worms co-expressing ARX-2::TagRFP (an essential subunit of the ARP-2/3 complex) at its endogenous locus, and CDC-42::GFP, expressed exogenously under the native *cdc-42* promoter (Neukomm *et al*, 2014; Wu *et al*, 2017). In control animals maintained on *E. coli*, both CDC-42 and ARX-2 localized predominantly to the apical membrane of the enterocytes, with little accumulation in the cytoplasm over 2 days of exposure (Fig. 2D and 2G; OP50 panel and Fig. S2C). Upon exposure to *P. aeruginosa*, both cytoplasmic and apical CDC-42 levels increased markedly (Fig. 2D enlarged ROI, 2E and 2F). Cytoplasmic levels of ARX-2 also increased (~2.6 fold) (Fig. 2H) though apical ARX-2 remained unchanged relative to *E. coli* (Fig. 2I). Intracellular actin mirrored that of ARX-2, with ~2.5 fold increase in cytoplasmic levels but none in apical levels (Fig. 2J- 2L). Surprisingly, Phalloidin-AlexaFluor647 staining and LifeACT::mRuby did not show any cytoplasmic staining, suggesting that the enhanced cytoplasmic actin pool following *P. aeruginosa* infection might represent filamentous actin (Fig. S1F-S1H). Thus, the increased cytoplasmic levels following *P. aeruginosa* infection reflects accumulation of G-actin rather than loss of F-actin from the apical surface.

P. aeruginosa **induced disruption of cortical actin results in apical surface deformation**

It seemed counterintuitive that apical ARX-2 and ACT-5 intensities did not increase despite CDC-42 enrichment. To clarify this conundrum, we measured apical levels of ACT-5 and ARX-2 in *cdc-42(RNAi)* worms, and found them to be significantly reduced (see OP50 panels in Figs. 3A, S3A, S3B and S3D). Thus apical actin and ARP-2/3

232 complex are sensitive to CDC-42-depletion, but not to *P. aeruginosa* induced CDC-
233 42-enrichment. The absence of deformation in *cdc-42(RNAi)* animals could therefore
234 reflect a direct effect of CDC-42 depletion or an indirect effect via reduced ARP-2/3-
235 mediated F-actin polymerization. To distinguish these, we depleted ACT-5 or ARX-2
236 in worms co-expressing CDC-42::GFP and ARX-2::TagRFP. Due to *act-5(RNAi)*-
237 associated developmental defects, analyses were restricted to day 1 post-infection.
238 Strikingly, *act-5(RNAi)* and *arx-2(RNAi)* worms, like *cdc-42(RNAi)* showed rescue of
239 deformation phenotype following infection despite elevated CDC-42 levels (red open
240 arrowheads in Fig.3C-E,3G and S3E).

241 To probe the function of ARP-2/3 dependent actin polymerization in *P. aeruginosa*
242 induced intestinal deformation, we analysed worms co-expressing mCherry::ACT5
243 and an apical membrane maker, PGP-1::GFP. In control worms fed with *E. coli*, ACT-
244 5 and PGP-1 were uniformly co-localized at apical surface (Fig. 3F; control panel). In
245 *arx-2(RNAi)* intestines, apical actin was absent and instead appeared as cytoplasmic
246 aggregates, even when fed with *E. coli* (Fig. 3F; *arx-2(RNAi)* red filled arrowheads).
247 This ruled out cytoplasmic actin accumulation as a possible cause of *P. aeruginosa*-
248 induced deformation. ARP-2/3 disruption has been implicated in cytoplasmic
249 mislocalization of membrane bound components such as DLG-1 and ERM-1
250 (Bernadskaya *et al*, 2011). PGP-1 displayed diffused apical localization in *arx-2(RNAi)*
251 intestines (Fig. 3F; *arx-2(RNAi)* red hollow arrowheads). These results suggested the
252 central role of ARP-2/3 polymerized actin in maintenance of apical membrane
253 organization. Importantly, CDC-42 and ARX-2 maintained apical localization even in
254 the absence of actin (Fig. 3F and 3G), confirming their upstream role in the actin
255 polymerization pathway. Collectively, these results demonstrate that rescue of apical
256 deformation in *cdc-42(RNAi)* and *arx-2(RNAi)* intestines following *P. aeruginosa*
257 exposure was due to disruption of ARP-2/3 mediated actin polymerization.

258

259 **Fragmented ARP-2/3 clustering and F-actin disorganization drives release of**
260 **membrane vesicles into the intestinal lumen following *P. aeruginosa* exposure.**

261 Although overall intensities of apical ARX-2 and ACT-5 were comparable between
262 worms exposed to *P. aeruginosa* and *E. coli* (Fig. 2I and 2L), their surface localization

263 patterns were markedly distinct. In *E. coli*-fed worms, ARX-2 was evenly distributed at
264 the apical surface (Fig. 4A; OP50, cyan arrowhead) essential for contiguous actin
265 polymerization, supporting brush border integrity (Bidaud-Meynard *et al*, 2021;
266 MacQueen *et al*, 2005b; Stutz *et al*, 2015). In contrast, *P. aeruginosa*-infected animals
267 exhibited fragmented ARX-2 clusters, interspersed with ARX-2-depleted regions (Fig.
268 4A; PA14, white arrows). We sought to correlate the cortical actin distribution with this
269 fragmented ARP-2/3 localization using worms co-expressing mCherry::ACT-5 and
270 ARX-2::GFP. Medial confocal sections of intestines from this strain when exposed to
271 *P. aeruginosa* resulted in apical actin to protrude as a 'bud-like' structure into the
272 lumen, emerging from ARX-2-free apical surface (Fig 4B; actin protrusions - yellow
273 arrowheads, fragmented ARP-2/3 – cyan arrows and Fig. 1C; red arrows in enlarged
274 ROI). By day-2, these protrusions pinched off as vesicles, coinciding with apical
275 surface deformation (Fig. 1C; day-2 PA14 panel - red arrows in enlarged ROI and Fig.
276 4D). Lattice light sheet microscopy of the intestinal lumen surface of animals
277 expressing mCherry::ACT-5 exposed to *P. aeruginosa* expressing GFP revealed
278 extracellular pinching of actin rich vesicles from the apical surface into the lumen (Fig.
279 4C; enlarged ROI, cyan arrows).

280 To determine whether these extracellular actin structures were membrane-enclosed,
281 we examined worms co-expressing mCherry::ACT-5 and PGP-1::GFP. Medial
282 confocal images on day-2 post-infection revealed apical buds at various stages: initial
283 protrusion (Fig. 4D; ROIs 1a & 2a), membrane pinching (1b & 2b), and free vesicles
284 in the lumen (cyan arrows, 1c & 2c). Intensity line-scan analysis confirmed that these
285 vesicles consisted of cortical actin cores surrounded by PGP-1::GFP-labelled apical
286 membrane. LifeACT::mRuby labeled these vesicles, indicating filamentous actin
287 content (Fig. 4E). Diameter of actin containing vesicles was ~ 0.59 μm (Fig. 4E). These
288 results support the view that *P. aeruginosa* exposure led to disordered ARP-2/3
289 localization at the apical lumen surface destabilising cortical actin organization,
290 resulting in the release of F-actin rich vesicles from the apical surface into lumen.

291

292 ***P. aeruginosa* infection disrupts apical polarity of enterocyte epithelium**

293 Fragmented ARP-2/3 clustering and vesicle shedding suggested a loss of apical
294 membrane identity. *P. aeruginosa* attachment to MDCK cells triggers a transient
295 PI(3,4,5)P_3 accumulation at the apical surface resulting in the loss of apical membrane
296 identity (Kierbel *et al*, 2007, 2005; Thuenauer *et al*, 2022). To check if *P. aeruginosa*
297 might cause a similar disruption to the polarity in *C. elegans* intestinal epithelium, we
298 analysed the localization of the *C. elegans* Scribble homolog, LET-413 and the cell
299 junction marker, DLG-1. The LET-413 complex and DLG-1 have been reported to be
300 essential for maintenance of basolateral domains in *C. elegans* by regulating the
301 localization of apical polarity components (Bossinger *et al*, 2004; McMahon *et al*,
302 2001). In *E. coli*-fed worms, the localization of LET-413 was limited to the basolateral
303 membrane with the apical surface largely devoid of any LET-413 (Fig. 5A; OP50 panel,
304 basolateral surface -yellow filled arrowhead, apical surface -yellow asterisks) (Legouis
305 *et al*, 2000). Upon exposure to *P. aeruginosa,* we observed a significant increase in
306 LET-413 levels along the apical and lateral membranes (Fig. 5A; PA14 panel, apical
307 surface - yellow arrows, lateral membrane- yellow open arrowhead, 5B and 5C),
308 indicating disruption in cell polarity. *P. aeruginosa* infection did not affect the position
309 of cell junctions (AJ)(Fig. 5A; cyan arrows).

310 The absence of intestinal deformation in *cdc-42(RNAi)* animals prompted us to
311 investigate if CDC-42 might also regulate apico-lateral polarity following *P. aeruginosa*
312 exposure. To this end, we checked the localization of LET-413 in control (L4440) and
313 *cdc-42(RNAi)* worms. The enhanced apical localization of LET-413 in the intestines of
314 control (L4440) worms was significantly diminished in *cdc-42(RNAi)* animals following
315 *P. aeruginosa* exposure (Fig. 5D). Conversely, we did not detect any disturbance to
316 the apical localization of CDC-42 and ARP-2/3 in *let-413(RNAi)* intestines, in
317 agreement with previous reports indicating that LET-413 depletion has minimal effect
318 on epithelial polarity (Fig S5A) (Riga *et al*, 2021). Moreover, similar to control animals,
319 *P. aeruginosa* exposure to *let-413(RNAi)* worms resulted in apical surface deformation
320 as well as elevated cytoplasmic levels of CDC-42 (S5A and S5B). Taken together,
321 these results suggest that upon exposure to *P. aeruginosa,* the apical surface *C.*
322 *elegans* intestine acquires basolateral characteristics in a CDC-42-dependent
323 mechanism.

324

325 **PI3K-AKT pathway depletion abrogates *P. aeruginosa* induced CDC-42 mis-**
326 **localization and intestinal deformation**

327 Disruption of the PI3K-AKT pathway impedes *P. aeruginosa* infection in MDCK cells
328 (Kierbel *et al*, 2005). Similarly, long-lived *C. elegans* mutants such as *akt-1*, *akt-2* and
329 *age-1*/PI3K exhibit resistance to *P. aeruginosa* (Evans *et al*, 2008; Garsin *et al*, 2003).
330 Our observation that *P. aeruginosa* disrupted intestinal polarity in *C. elegans*
331 suggested that host response to *P. aeruginosa* infection could be conserved between
332 mammalian epithelium and *C. elegans* enterocytes. To examine the conservation in
333 cellular response to *P. aeruginosa* between mammmals and *C. elegans*, we
334 diminished PI3K-AKT signalling by a simultaneous depletion of AKT-1 and AKT-2
335 using RNAi and checked the localizations of LET-413, CDC-42 and ARX-2 in the
336 intestines of *C elegans*. Depletion of AKT-1/AKT-2, like in *cdc-42(RNAi)* worms,
337 prevented the apical localization of LET-413 following *P. aeruginosa* infection (Fig.
338 5D). Evidence for crosstalk between CDC-42 dependent actin assembly and PI3K-
339 AKT in mammalian cells prompted us to measure CDC-42 and ARX-2 levels in the
340 intestines of *akt-1(RNAi)+akt-2(RNAi)* and *age-1(RNAi)* animals following *P.*
341 *aeruginosa* exposure (McCormick *et al*, 2019; Yang *et al*, 2012). Intestinal epithelium
342 of animals depleted of AKT or AGE-1 displayed diminished apical and cytosolic ARX-
343 2 localization compared to control animals (Fig. 5E, S5E - S5H), and also did not
344 display apical deformation following *P. aeruginosa* exposure (Fig. 5D). Taken
345 together our results suggest that PI3K activation induced apical enrichment of
346 PI(3,4,5)P_3 following exposure to *P. aeruginosa*, disrupts apical membrane polarity
347 and de-localizes ARP-2/3 dependent actin assembly from the apical surface resulting
348 in intestinal deformation. These results re-enforces the importance of polarity
349 disruption as a key event following *P. aeruginosa* infection and prior to intestinal
350 deformation.

351

352 **Extracellular localization of *Pseudomonas* is sufficient to induce intestinal**
353 **deformation**

354 *Pseudomonas aeruginosa* functions both as an extracellular and intracellular
355 pathogen infecting wide range of hosts (Resko *et al*, 2024). Transient activation of

356 PI3K pathway resulting in apical membrane acquiring basolateral characteristics was
357 resulted in internalization of *P. aeruginosa* by MDCK cells (Kierbel *et al*, 2005).
358 Electron microscopy studies of *P. aeruginosa* -infected *C. elegans* intestine have also
359 reported *Pseudomonas* invasion into enterocytes (Irazoqui *et al*, 2010; Xue *et al*,
360 2024). To determine whether intestinal deformation in *C. elegans* results from *P.*
361 *aeruginosa* breaching the epithelial barrier, we performed live confocal imaging of
362 infection using GFP-expressing *E. coli* or *P. aeruginosa*. Unlike E. coli (OP50-GFP),
363 which were in very few numbers even after two days of exposure, *P. aeruginosa*
364 (PA14-GFP) cells formed visible aggregates throughout the intestinal lumen as early
365 as one-day post infection (Fig. 6A). Interestingly, apical surfaces adjacent to these
366 aggregates displayed mild contortions, which progressed into pronounced
367 deformation by day 2 (Fig. 6A; red triangles in bottom row-PA14). Orthogonal
368 reconstruction (YZ plane) of confocal (XY) planes revealed that PA14-GFP localization
369 remained restricted to the lumen with no detectable signal in the cytoplasm of the
370 intestinal cells (Fig.6A; PA14 panel). These observations were confirmed using lattice
371 light-sheet microscopy (Fig. 4C and Supplementary Movie S1). To test whether apical
372 surface deformation is a general enterocyte response to any pathogen, we conducted
373 parallel infection assays using *Salmonella enterica* serovar *typhimurium* (Stm), a
374 Gram-negative bacterium known to modulate CDC-42 activity during mammalian
375 infections (Bandyopadhyay *et al*, 2024) and cause lethality in *C. elegans (*Fig. S6A)
376 (Aballay *et al*, 2000; Desai *et al*, 2019). Stm-GFP infection in worms expressing
377 mCherry::ACT-5, resulted in efficient intestinal colonization by day 2 similar to *P.*
378 *aeruginosa* (Fig. S5B). However, despite this robust lumen colonization, in contrast to
379 *P. aeruginosa* , Stm-exposed intestines did not display any surface deformation (Fig.
380 6A; middle row, yellow open arrowheads). Taken together these results indicate that
381 the intestinal deformation is a pathogen specific response by the *C. elegans*
382 enterocyte to extracellular *Pseudomonas* infection.

383

384 **Physical association between live *P .aeruginosa* and the intestinal surface is not**
385 **essential for apical deformation**

386 Given the key role for physical association with host cells in *P. aeruginosa*
387 pathogenesis (via various adhesins, including flagella, type IV pili, type III secretion
388 system (T3SS), and lectins (Bucior *et al*, 2012; Comolli *et al*, 1999; Thuenauer *et al*,
389 2022), we asked whether a direct attachment of *P. aeruginosa* to the apical membrane
390 of *C. elegans* intestine was necessary to trigger tissue deformation. First, we tested if
391 exposure to live microbes is essential for inducing deformation of apical surface, by
392 exposing animals to heat-killed *E. coli* or *P. aeruginosa* instead of live bacteria. Since
393 worms displayed no noticeable defects in growth, maturation or egg laying, we
394 concluded that heat-killed bacteria as food source was not nutritionally limiting.
395 However, unlike live *P. aeruginosa*, heat killed *P. aeruginosa* failed to induce intestinal
396 deformation (Fig. 6B; open triangle). Our observation agrees with previous reports
397 showing heat-killed *P. aeruginosa* does not elicit immune response in *C.* elegans
398 (Irazoqui *et al*, 2010). Since extracellular *P. aeruginosa* induces intestinal deformation,
399 we hypothesized that secreted factors may mediate this effect. To test this, we
400 exposed worms to cell-free filter sterilized supernatant collected from *P. aeruginosa* or
401 *E. coli* cultures. Remarkably, a 12-hour exposure to *P. aeruginosa* supernatant alone
402 was sufficient to trigger apical surface deformation in the *C. elegans* intestine (Fig.
403 6C).

404 The global response regulator, GacA governs the expression of numerous virulence
405 factors secreted by *P. aeruginosa,* including toxins and components in biofilm
406 regulation (Barta *et al*, 1992; Kitten *et al*, 1998; Parkins *et al*, 2001; Reimmann *et al*,
407 1997) and has also been implicated in inducing developmental defects and activating
408 the unfolded protein response (UPR) in *C. elegans* intestinal epithelium (Pellegrino *et*
409 *al*, 2014). To assess the role of GacA in apical surface deformation, we exposed
410 mCherry::ACT-5-expressing worms to *E. coli*, *P. aeruginosa* or a *gacA* deletion mutant
411 (PA14*ΔgacA*) strain. The intestines of worms exposed to PA14*ΔgacA* exhibited an
412 intermediate level of intestinal deformation compared to those infected with wild-type
413 PA14 (Fig. 6D and 6E). Importantly, a *gacA* deletion mutant (PA14*ΔgacA*) retains
414 partial pathogenicity, causing ~50% lethality in infected worms (Fig. 6F) (Feinbaum *et*
415 *al*, 2012; Tan *et al*, 1999b). These results suggest that while GacA partially contributes
416 to *P. aeruginosa* pathogenesis in *C. elegans*, a GacA-independent mechanism also
417 exists, through which the pathogen elicits tissue surface deformation. Taken together,

418 these results support the view that while intestinal distension is a general tissue
419 response to microbial colonization of the lumen, mechanical deformation of apical
420 surface is a specific response to extracellular heat labile component from *P.*
421 *aeruginosa*.

422

423 **DISCUSSION**

424 Here we report that *P. aeruginosa* exposure induces two distinct morphological
425 alterations in the *C. elegans* intestine; (a) lumenal distension, reflected by increased
426 intestinal width, and (b) deformation of the apical surface, seen as wrinkling of the
427 lumen. While lumen distension has been previously been described as a general
428 response to microbial colonisation, we show that apical surface deformation is specific
429 to *P. aeruginosa* infection.

430 *P. aeruginosa* infection in MDCK cells recruits PI3K to the attachment sites, causing
431 PIP_3 enrichment, apical mislocalization of basolateral proteins, and disruption of
432 epithelial polarity through perturbation of the Rho GTPases - RHO-1, RAC-1 and CDC-
433 42 (Aktories, 2011; Kazmierczak & Engel, 2002; Kierbel *et al*, 2007; Krall *et al*, 2000).
434 Consistent with this, we find that inhibition of either PI3K-AKT signalling or CDC-42-
435 dependent actin assembly completely abolished both intestinal deformation and
436 pathogen-induced lethality. *P. aeruginosa* infection also led to apical mis-localization
437 of the basolateral marker LET-413, indicating a loss of apical membrane identity,
438 though no apical markers were mislocalized baso-laterally. The rescue observed in
439 *cdc-42(RNAi)* animals further implicated CDC-42 in pathogen-induced actin
440 remodelling. However, depletion of the downstream polarity facrot, LET-413 failed to
441 rescue deformation, suggesting that CDC-42 contributes primarily via actin assembly
442 rather than polarity regulation. Supporting this, depletion of ACT-5 or disruption of
443 ARP-2/3 phenocopied *cdc-42(RNAi)*. In line with previous reports (Kierbel *et al*, 2005;
444 Paradis & Ruvkun, 1998), we noted that attenuation of PI3K-AKT signalling rescued
445 the intestinal deformation by limiting disruption in CDC-42 dependent ARP-2/3 mis-
446 localization. These results highlights the central role of CDC-42-ARP-2/3-mediated
447 actin polymerization in *P. aeruginosa* induced deformation.

448 In uninfected animals, ARP-2/3, together with actin-binding proteins such as PLST-1
449 and FLN-2, forms evenly distributed apical clusters (Bidaud-Meynard *et al*, 2021).
450 ARP-2/3 polymerizes contiguous F-actin to support microvillar structures (Fig. 4A).
451 Infection by *P. aeruginosa* fragmented these clusters, disrupting local actin
452 organization, destabilizing the apical surface, which promoted vesiculation of actin-
453 rich membrane into the lumen. Because actin structures in enterocytes show minimal
454 mobility, their disruption cannot be rapidly replenished, destabilizing the surface
455 (Bernadskaya *et al*, 2011; Bidaud-Meynard *et al*, 2021) (Fig. 6G). This agrees with
456 electron micrographs showing actin protrusions in MDCK cells (Kierbel *et al*, 2005) as
457 well as microvillar loss and accumulation of host debris in the *C. elegans* lumen during
458 infection (Irazoqui *et al*, 2010; Xue *et al*, 2024). Intriguingly, depletion of ARX-2 or
459 ACT-5 prevented vesicle release and surface deformation. We speculate that a
460 uniform depletion of ARP-2/3 or actin reduces actin availability for vesiculation. Similar
461 protection has been reported in MDCK cells, where Latrunculin A mediated actin
462 depolymerization attenuated *P. aeruginosa* infection by upto 60-fold (Kazmierczak *et*
463 *al*, 2004). CDC-42 upregulation and activation have been reported in polarized MDCK
464 cells (Kazmierczak *et al*, 2004). Consistent with these findings, *P. aeruginosa* infection
465 in *C. elegans* enterocytes led to cytoplasmic accumulation of CDC-42, ARP-2/3 and
466 actin. While RHO-mediated actin regulation and homeostasis are monitored in
467 mammals by pyrin- and NOD-dependent pathways, no equivalent surveillance been
468 reported in *C. elegans* (Mostowy & Shenoy, 2015). Although cytoplasmic actin
469 accumulation correlated with infection, it did not directly cause deformation. Whether
470 it may be sensed as a pattern of pathogenesis is remains to be addressed. Moreover,
471 MAPK signalling remained intact in *cdc-42(RNAi)* animals following infection,
472 indicating that CDC-42 depletion does not impair microbial sensing.

473 Similar to polarized MDCK cells, *P. aeruginosa* does not breach the cell membrane
474 of *C. elegans* epithelium. Additionally, while the surface deformation phenotype could
475 be recapitulated by exposure to cell-free supernatant from *P . aeruginosa* growth
476 culture but not by heat-killed bacteria suggested the role of a heat-labile factor. Given
477 the extracellular lifestyle of *P. aeruginosa* in polarized epithelia, extracellular
478 membrane vesicles (OMVs) rich in surface components, quorum-sensing molecules ,

toxins and other virulence factors, are plausible mediators of deformation signal (Bauman & Kuehn, 2009, 2006; Kuehn & Kesty, 2005; Mashburn & Whiteley, 2005).

Pseudomonas is generally considered as an extracellular pathogen and its intracellular lifestyle is usually associated with tissue injury. While *P. aeruginosa* has been shown to infiltrate the cytoplasmic space many host systems, we have not observed epithelial breach in our experiments in *C. elegans* intestine. We demonstrate that extracellular *P. aeruginosa* exploits PI3K-AKT activation to perturb CDC-42-ARP-2/3-mediated actin organization leading to loss of apical polarity and cytoskeletal integrity in the *C. elegans* enterocytes. Our findings reveal an evolutionarily conserved strategy by which *P. aeruginosa* subverts actin regulation during extracellular infection. We propose that the pathogen mediated disruption of polarity impairs apically directed transport and secretion of antimicrobial peptides, and surface binding lectins. An attenuated antimicrobial response could allow bacterial proliferation in the lumen and a rapid spreading of the bacteria in the population.

ACKNOWLEDGEMENTS

This work was supported by DBT-Wellcome India Alliance Fellowship (IA/I/18/1/503624) and ANRF Core research grant (CRG/2023/004638) to A.P, Department of Biotechnology Junior research Fellowship (DBT/2024-25/AshokaUni/2486) to T.S., and core funding support from the Trivedi School of Biosciences, Ashoka University. We acknowledge the infrastructure support from the Central Bio-imaging facility and Ashoka-Zeiss Core Imaging Facility at Ashoka University. We thank Ms. Megha Rai for help with vesicle size quantification, Ms. Shraddha Nirmal for assisting with generating strains for some of the experiments and Ms. Purna Pardeshi for some of the schematic images in this manuscript. We are grateful to the labs of Arnab Mukhopadhyay, Anindya Ghosh-Roy, Emily Troemel, Grégoire Michaux, Jogender Singh, Mike Boxem, Mahak Sharma and Varsha Singh, for sharing *C. elegans* and bacterial strains. Some strains were provided by the CGC, which is funded by NIH Office of Research Infrastructure Programs (P40OD010440). We thank Jogender Singh for discussions.

AUTHOR CONTRIBUTIONS**:** D.A.N and A.P conceived the project. D.A.N, T.S and A.P designed the experiments. D.A.N and T.S performed experiments. D.A.N and T.S analysed the data with input from A.P. A.P wrote the manuscript with input from D.A.N and T.S.

References:

Aballay A, Yorgey P & Ausubel FM (2000) Salmonella typhimurium proliferates and establishes a persistent infection in the intestine of Caenorhabditis elegans. *Curr Biol* 10: 1539–1542

Aktories K (2011) Bacterial protein toxins that modify host regulatory GTPases. *Nat Rev Microbiol* 9: 487–498

Ann Mack N & Georgiou M (2014) The interdependence of the Rho GTPases and apicobasal cell polarity. *Small GTPases* 5: 37–41

Armenti ST & Nance J (2012) Adherens junctions in C. elegans embryonic morphogenesis. *Subcell Biochem* 60: 279–299

Balla KM & Troemel ER (2013) Caenorhabditis elegans as a model for intracellular pathogen infection. *Cell Microbiol* 15: 1313–1322

Bandyopadhyay S, Zhang X, Ascura A, Edelblum KL, Bonder EM & Gao N (2024) Salmonella engages CDC42 effector protein 1 for intracellular invasion. *J Cell Physiol* 239

Barta TM, Kinscherf TG & Willis DK (1992) Regulation of tabtoxin production by the lemA gene in Pseudomonas syringae. *J Bacteriol* 174: 3021–3029

Bastounis EE, Radhakrishnan P, Prinz CK & Theriot JA (2022) Mechanical Forces Govern Interactions of Host Cells with Intracellular Bacterial Pathogens. *Microbiol Mol Biol Rev* 86: e00094-20

Bauman SJ & Kuehn MJ (2006) Purification of outer membrane vesicles from Pseudomonas aeruginosa and their activation of an IL-8 response. *Microbes Infect* 8: 2400–2408

Bauman SJ & Kuehn MJ (2009) Pseudomonas aeruginosa vesicles associate with and are internalized by human lung epithelial cells. *BMC Microbiol* 9: 26

Berg M, Stenuit B, Ho J, Wang A, Parke C, Knight M, Alvarez-Cohen L & Shapira M (2016) Assembly of the *Caenorhabditis elegans* gut microbiota from diverse soil microbial environments. *ISME J* 10: 1998–2009

Bernadskaya YY, Patel FB, Hsu HT & Soto MC (2011) Arp2/3 promotes junction formation and maintenance in the Caenorhabditis elegans intestine by regulating membrane association of apical proteins. *Mol Biol Cell* 22: 2886–2899

Bidaud-Meynard A, Demouchy F, Nicolle O, Pacquelet A, Suman SK, Plancke CN, Robin FB & Michaux G (2021) High-resolution dynamic mapping of the *C. elegans* intestinal brush border. *Development* 148

549 Bollen DP, Reddy KC, Lascarez-Lagunas LI, Kim DH & Colaiácovo MP (2024) Germline
550 mitotic quiescence and cell death are induced in *Caenorhabditis elegans* by
551 exposure to pathogenic *Pseudomonas aeruginosa*. *GENETICS* 226: iyad197

552 Bossinger O, Fukushige T, Claeys M, Borgonie G & McGhee JD (2004) The apical
553 disposition of the Caenorhabditis elegans intestinal terminal web is maintained
554 by LET-413. *Dev Biol* 268: 448–456

555 Bucior I, Pielage JF & Engel JN (2012) Pseudomonas aeruginosa Pili and Flagella Mediate
556 Distinct Binding and Signaling Events at the Apical and Basolateral Surface of
557 Airway Epithelium. *PLoS Pathog* 8: e1002616

558 Cohen LB & Troemel ER (2015) Microbial pathogenesis and host defense in the
559 nematode C. elegans. *Curr Opin Microbiol* 23: 94–101

560 Colonne PM, Winchell CG & Voth DE (2016) Hijacking Host Cell Highways: Manipulation
561 of the Host Actin Cytoskeleton by Obligate Intracellular Bacterial Pathogens.
562 *Front Cell Infect Microbiol* 6

563 Comolli JC, Waite LL, Mostov KE & Engel JN (1999) Pili Binding to Asialo-GM1 on
564 Epithelial Cells Can Mediate Cytotoxicity or Bacterial Internalization by
565 *Pseudomonas aeruginosa*. *Infect Immun* 67: 3207–3214

566 Cowell BA, Evans DJ & Fleiszig SMJ (2005) Actin cytoskeleton disruption by ExoY and its
567 effects on *Pseudomonas aeruginosa* invasion. *FEMS Microbiol Lett* 250: 71–76

568 Desai SK, Padmanabhan A, Harshe S, Zaidel-Bar R & Kenney LJ (2019) Salmonella
569 biofilms program innate immunity for persistence in Caenorhabditis elegans.
570 *Proc Natl Acad Sci U S A* 116: 12462–12467

571 Dimov I & Maduro MF (2019) The C. elegans intestine: organogenesis, digestion, and
572 physiology. *Cell Tissue Res* 377: 383–396

573 Dunbar TL, Yan Z, Balla KM, Smelkinson MG & Troemel ER (2012) C. elegans detects
574 pathogen-induced translational inhibition to activate immune signaling. *Cell*
575 *Host Microbe* 11: 375–386

576 Egge N, Arneaud SLB, Wales P, Mihelakis M, McClendon J, Fonseca RS, Savelle C,
577 Gonzalez I, Ghorashi A, Yadavalli S, *et al* (2019) Age-Onset Phosphorylation of a
578 Minor Actin Variant Promotes Intestinal Barrier Dysfunction. *Dev Cell* 51: 587-
579 601.e7

580 Estes KA, Dunbar TL, Powell JR, Ausubel FM & Troemel ER (2010) bZIP transcription
581 factor zip-2 mediates an early response to Pseudomonas aeruginosa infection in
582 Caenorhabditis elegans. *Proc Natl Acad Sci U S A* 107: 2153–2158

583 Evans EA, Chen WC & Tan M (2008) The DAF-2 insulin-like signaling pathway
584 independently regulates aging and immunity in *C. elegans*. *Aging Cell* 7: 879–893

585 Ewbank J (2006) Signaling in the immune response. *WormBook*

Feinbaum RL, Urbach JM, Liberati NT, Djonovic S, Adonizio A, Carvunis A-R & Ausubel FM (2012) Genome-Wide Identification of Pseudomonas aeruginosa Virulence-Related Genes Using a Caenorhabditis elegans Infection Model. *PLoS Pathog* 8: e1002813

Filipowicz A, Lalsiamthara J & Aballay A (2021) TRPM channels mediate learned pathogen avoidance following intestinal distention. *eLife* 10: e65935

Fleiszig SM, Evans DJ, Do N, Vallas V, Shin S & Mostov KE (1997) Epithelial cell polarity affects susceptibility to Pseudomonas aeruginosa invasion and cytotoxicity. *Infect Immun* 65: 2861–2867

Garsin DA, Villanueva JM, Begun J, Kim DH, Sifri CD, Calderwood SB, Ruvkun G & Ausubel FM (2003) Long-Lived *C. elegans daf-2* Mutants Are Resistant to Bacterial Pathogens. *Science* 300: 1921–1921

Geisler F, Coch RA, Richardson C, Goldberg M, Bevilacqua C, Prevedel R & Leube RE (2020) Intestinal intermediate filament polypeptides in C. elegans: Common and isotype-specific contributions to intestinal ultrastructure and function. *Sci Rep* 10: 3142

Göbel V, Barrett PL, Hall DH & Fleming JT (2004) Lumen morphogenesis in C. elegans requires the membrane-cytoskeleton linker erm-1. *Dev Cell* 6: 865–873

Gravato-Nobre MJ, Nicholas HR, Nijland R, O'Rourke D, Whittington DE, Yook KJ & Hodgkin J (2005) Multiple genes affect sensitivity of Caenorhabditis elegans to the bacterial pathogen Microbacterium nematophilum. *Genetics* 171: 1033–1045

Irazoqui JE, Troemel ER, Feinbaum RL, Luhachack LG, Cezairliyan BO & Ausubel FM (2010) Distinct Pathogenesis and Host Responses during Infection of C. elegans by P. aeruginosa and S. aureus. *PLoS Pathog* 6: e1000982

Jaffe AB & Hall A (2005) Rho GTPases: Biochemistry and biology. *Annu Rev Cell Dev Biol* 21: 247–269

Kazmierczak BI & Engel JN (2002) *Pseudomonas aeruginosa* ExoT Acts In Vivo as a GTPase-Activating Protein for RhoA, Rac1, and Cdc42. *Infect Immun* 70: 2198–2205

Kazmierczak BI, Mostov K & Engel JN (2004) Epithelial Cell Polarity Alters Rho-GTPase Responses to *Pseudomonas aeruginosa*. *Mol Biol Cell* 15: 411–419

Kierbel A, Gassama-Diagne A, Mostov K & Engel JN (2005) The Phosphoinositol-3-Kinase–Protein Kinase B/Akt Pathway Is Critical for *Pseudomonas aeruginosa* Strain PAK Internalization. *Mol Biol Cell* 16: 2577–2585

Kierbel A, Gassama-Diagne A, Rocha C, Radoshevich L, Olson J, Mostov K & Engel J (2007) *Pseudomonas aeruginosa* exploits a PIP3-dependent pathway to transform apical into basolateral membrane. *J Cell Biol* 177: 21–27

Kitten T, Kinscherf TG, McEvoy JL & Willis DK (1998) A newly identified regulator is required for virulence and toxin production in Pseudomonas syringae. *Mol Microbiol* 28: 917–929

Krall R, Schmidt G, Aktories K & Barbieri JT (2000) Pseudomonas aeruginosa ExoT is a Rho GTPase-activating protein. *Infect Immun* 68: 6066–6068

Kuehn MJ & Kesty NC (2005) Bacterial outer membrane vesicles and the host–pathogen interaction. *Genes Dev* 19: 2645–2655

Kumar S, Egan BM, Kocsisova Z, Schneider DL, Murphy JT, Diwan A & Kornfeld K (2019) Lifespan Extension in C. elegans Caused by Bacterial Colonization of the Intestine and Subsequent Activation of an Innate Immune Response. *Dev Cell* 49: 100-117.e6

Kuss-Duerkop SK & Keestra-Gounder AM (2020) NOD1 and NOD2 Activation by Diverse Stimuli: a Possible Role for Sensing Pathogen-Induced Endoplasmic Reticulum Stress. *Infect Immun* 88: e00898-19

Legouis R, Gansmuller A, Sookhareea S, Bosher JM, Baillie DL & Labouesse M (2000) LET-413 is a basolateral protein required for the assembly of adherens junctions in Caenorhabditis elegans. *Nat Cell Biol* 2: 415–422

Lei M, Tan Y, Tu H & Tan W (2024) Neuronal basis and diverse mechanisms of pathogen avoidance in Caenorhabditis elegans. *Front Immunol* 15: 1353747

Ma L, Rohatgi R & Kirschner MW (1998) The Arp2/3 complex mediates actin polymerization induced by the small GTP-binding protein Cdc42. *Proc Natl Acad Sci U S A* 95: 15362–15367

MacQueen AJ, Baggett JJ, Perumov N, Bauer RA, Januszewski T, Schriefer L & Waddle JA (2005a) ACT-5 Is an Essential *Caenorhabditis elegans* Actin Required for Intestinal Microvilli Formation. *Mol Biol Cell* 16: 3247–3259

MacQueen AJ, Baggett JJ, Perumov N, Bauer RA, Januszewski T, Schriefer L & Waddle JA (2005b) ACT-5 Is an Essential *Caenorhabditis elegans* Actin Required for Intestinal Microvilli Formation. *Mol Biol Cell* 16: 3247–3259

Mahajan-Miklos S, Tan M-W, Rahme LG & Ausubel FM (1999) Molecular Mechanisms of Bacterial Virulence Elucidated Using a Pseudomonas aeruginosa–Caenorhabditis elegans Pathogenesis Model. *Cell* 96: 47–56

Martin-Belmonte F, Gassama A, Datta A, Yu W, Rescher U, Gerke V & Mostov K (2007) PTEN-Mediated Apical Segregation of Phosphoinositides Controls Epithelial Morphogenesis through Cdc42. *Cell* 128: 383–397

Mashburn LM & Whiteley M (2005) Membrane vesicles traffic signals and facilitate group activities in a prokaryote. *Nature* 437: 422–425

McCormick B, Chu JY & Vermeren S (2019) Cross-talk between Rho GTPases and PI3K in the neutrophil. *Small GTPases* 10: 187–195

McEwan DL, Kirienko NV & Ausubel FM (2012) Host translational inhibition by Pseudomonas aeruginosa exotoxin A triggers an immune response in Caenorhabditis elegans. *Cell Host Microbe* 11: 364–374

McGhee J (2007) The C. elegans intestine. *WormBook*

McMahon L, Legouis R, Vonesch JL & Labouesse M (2001) Assembly of C. elegans apical junctions involves positioning and compaction by LET-413 and protein aggregation by the MAGUK protein DLG-1. *J Cell Sci* 114: 2265–2277

Melo JA & Ruvkun G (2012) Inactivation of conserved C. elegans genes engages pathogen- and xenobiotic-associated defenses. *Cell* 149: 452–466

Mostowy S & Shenoy AR (2015) The cytoskeleton in cell-autonomous immunity: structural determinants of host defence. *Nat Rev Immunol* 15: 559–573

Neukomm LJ, Zeng S, Frei AP, Huegli PA & Hengartner MO (2014) Small GTPase CDC-42 promotes apoptotic cell corpse clearance in response to PAT-2 and CED-1 in C. elegans. *Cell Death Differ* 21: 845–853

Paradis S & Ruvkun G (1998) *Caenorhabditis elegans* Akt/PKB transduces insulin receptor-like signals from AGE-1 PI3 kinase to the DAF-16 transcription factor. *Genes Dev* 12: 2488–2498

Parkins MD, Ceri H & Storey DG (2001) Pseudomonas aeruginosa GacA, a factor in multihost virulence, is also essential for biofilm formation. *Mol Microbiol* 40: 1215–1226

Pederson KJ, Vallis AJ, Aktories K, Frank DW & Barbieri JT (1999) The amino-terminal domain of *Pseudomonas aeruginosa* ExoS disrupts actin filaments via small-molecular-weight GTP-binding proteins. *Mol Microbiol* 32: 393–401

Pellegrino MW, Nargund AM, Kirienko NV, Gillis R, Fiorese CJ & Haynes CM (2014) Mitochondrial UPR-regulated innate immunity provides resistance to pathogen infection. *Nature* 516: 414–417

Pereira AG, Gracida X, Kagias K & Zhang Y (2020) *C. elegans* aversive olfactory learning generates diverse intergenerational effects. *J Neurogenet* 34: 378–388

Peterson ND, Icso JD, Salisbury JE, Rodríguez T, Thompson PR & Pukkila-Worley R (2022) Pathogen infection and cholesterol deficiency activate the C. elegans p38 immune pathway through a TIR-1/SARM1 phase transition. *eLife* 11: e74206

Peterson ND, Tse SY, Huang QJ, Wani KA, Schiffer CA & Pukkila-Worley R (2023) Non-canonical pattern recognition of a pathogen-derived metabolite by a nuclear hormone receptor identifies virulent bacteria in C. elegans. *Immunity* 56: 768-782.e9

Prakash D, Ms A, Radhika B, Venkatesan R, Chalasani SH & Singh V (2021) 1-Undecene from *Pseudomonas aeruginosa* is an olfactory signal for flight-or-fight response in *Caenorhabditis elegans*. *EMBO J* 40: e106938

Pukkila-Worley R & Ausubel FM (2012) Immune defense mechanisms in the Caenorhabditis elegans intestinal epithelium. *Curr Opin Immunol* 24: 3–9

Reimmann C, Beyeler M, Latifi A, Winteler H, Foglino M, Lazdunski A & Haas D (1997) The global activator GacA of Pseudomonas aeruginosa PAO positively controls the production of the autoinducer N-butyryl-homoserine lactone and the formation of the virulence factors pyocyanin, cyanide, and lipase. *Mol Microbiol* 24: 309–319

Resko ZJ, Suhi RF, Thota AV & Kroken AR (2024) Evidence for intracellular *Pseudomonas aeruginosa*. *J Bacteriol* 206

Riga A, Cravo J, Schmidt R, Pires HR, Castiglioni VG, Van Den Heuvel S & Boxem M (2021) Caenorhabditis elegans LET-413 Scribble is essential in the epidermis for growth, viability, and directional outgrowth of epithelial seam cells. *PLOS Genet* 17: e1009856

Ruch TR & Engel JN (2017) Targeting the Mucosal Barrier: How Pathogens Modulate the Cellular Polarity Network. *Cold Spring Harb Perspect Biol* 9: a027953

Sauvanet C, Wayt J, Pelaseyed T & Bretscher A (2015) Structure, Regulation, and Functional Diversity of Microvilli on the Apical Domain of Epithelial Cells. *Annu Rev Cell Dev Biol* 31: 593–621

Schulenburg H & Félix M-A (2017) The Natural Biotic Environment of*Caenorhabditis elegans*. *Genetics* 206: 55–86

Sepers JJ, Ramalho JJ, Kroll JR, Schmidt R & Boxem M (2022) ERM-1 Phosphorylation and NRFL-1 Redundantly Control Lumen Formation in the C. elegans Intestine. *Front Cell Dev Biol* 10

Shafaq-Zadah M, Brocard L, Solari F & Michaux G (2012) AP-1 is required for the maintenance of apico-basal polarity in the*C. elegans*intestine. *Development* 139: 2061–2070

Singh J & Aballay A (2019a) Microbial Colonization Activates an Immune Fight-and-Flight Response via Neuroendocrine Signaling. *Dev Cell* 49: 89-99.e4

Singh J & Aballay A (2019b) Intestinal infection regulates behavior and learning via neuroendocrine signaling. *eLife* 8: e50033

Stiernagle T (2006) Maintenance of C. elegans. *WormBook*

Stuart LM, Paquette N & Boyer L (2013) Effector-triggered versus pattern-triggered immunity: how animals sense pathogens. *Nat Rev Immunol* 13: 199–206

Stutz K, Kaech A, Aebi M, Künzler M & Hengartner MO (2015) Disruption of the C. elegans intestinal brush border by the fungal lectin CCL2 phenocopies dietary lectin toxicity in mammals. *PLoS ONE* 10: 1–23

Sun J & Barbieri JT (2004) ExoS Rho GTPase-activating Protein Activity Stimulates Reorganization of the Actin Cytoskeleton through Rho GTPase Guanine Nucleotide Disassociation Inhibitor. *J Biol Chem* 279: 42936–42944

Szumowski SC, Estes KA, Popovich JJ, Botts MR, Sek G & Troemel ER (2016) Small GTPases promote actin coat formation on microsporidian pathogens traversing the apical membrane of*Caenorhabditis elegans*intestinal cells: Actin coats on microsporidia-containing vesicles. *Cell Microbiol* 18: 30–45

Tan MW, Mahajan-Miklos S & Ausubel FM (1999a) Killing of Caenorhabditis elegans by Pseudomonas aeruginosa used to model mammalian bacterial pathogenesis. *Proc Natl Acad Sci U S A* 96: 715–720

Tan M-W, Rahme LG, Sternberg JA, Tompkins RG & Ausubel FM (1999b) *Pseudomonas aeruginosa* killing of *Caenorhabditis elegans* used to identify *P. aeruginosa* virulence factors. *Proc Natl Acad Sci* 96: 2408–2413

Thuenauer R, Kühn K, Guo Y, Kotsis F, Xu M, Trefzer A, Altmann S, Wehrum S, Heshmatpour N, Faust B, *et al* (2022) The Lectin LecB Induces Patches with Basolateral Characteristics at the Apical Membrane to Promote Pseudomonas aeruginosa Host Cell Invasion. *mBio* 13: e00819-22

Tran CS, Eran Y, Ruch TR, Bryant DM, Datta A, Brakeman P, Kierbel A, Wittmann T, Metzger RJ, Mostov KE, *et al* (2014) Host Cell Polarity Proteins Participate in Innate Immunity to Pseudomonas aeruginosa Infection. *Cell Host Microbe* 15: 636–643

Tse-Kang S, Wani KA & Pukkila-Worley R (2025) Patterns of pathogenesis in innate immunity: insights from C. elegans. *Nat Rev Immunol*

Vance RE, Isberg RR & Portnoy DA (2009) Patterns of Pathogenesis: Discrimination of Pathogenic and Nonpathogenic Microbes by the Innate Immune System. *Cell Host Microbe* 6: 10–21

Winter JF, Höpfner S, Korn K, Farnung BO, Bradshaw CR, Marsico G, Volkmer M, Habermann B & Zerial M (2012) Caenorhabditis elegans screen reveals role of PAR-5 in RAB-11-recycling endosome positioning and apicobasal cell polarity. *Nat Cell Biol* 14: 666–676

Wu D, Chai Y, Zhu Z, Li W, Ou G & Li W (2017) CED-10-WASP-Arp2/3 signaling axis regulates apoptotic cell corpse engulfment in C. elegans. *Dev Biol* 428: 215–223

Xue F, Ragno M, Blackburn SA, Fasseas M, Maitra S, Liang M, Rai S, Mastroianni G, Tholozan F, Thompson R, *et al* (2024) New tools to monitor Pseudomonas aeruginosa infection and biofilms in vivo in C. elegans. *Front Cell Infect Microbiol* 14

Yang HW, Shin M-G, Lee S, Kim J-R, Park WS, Cho K-H, Meyer T & Do Heo W (2012) Cooperative Activation of PI3K by Ras and Rho Family Small GTPases. *Mol Cell* 47: 281–290

Zhang Y, Lu H & Bargmann CI (2005) Pathogenic bacteria induce aversive olfactory learning in Caenorhabditis elegans. *Nature* 438: 179–184

Figure 1

Divyashree et. al (2025)

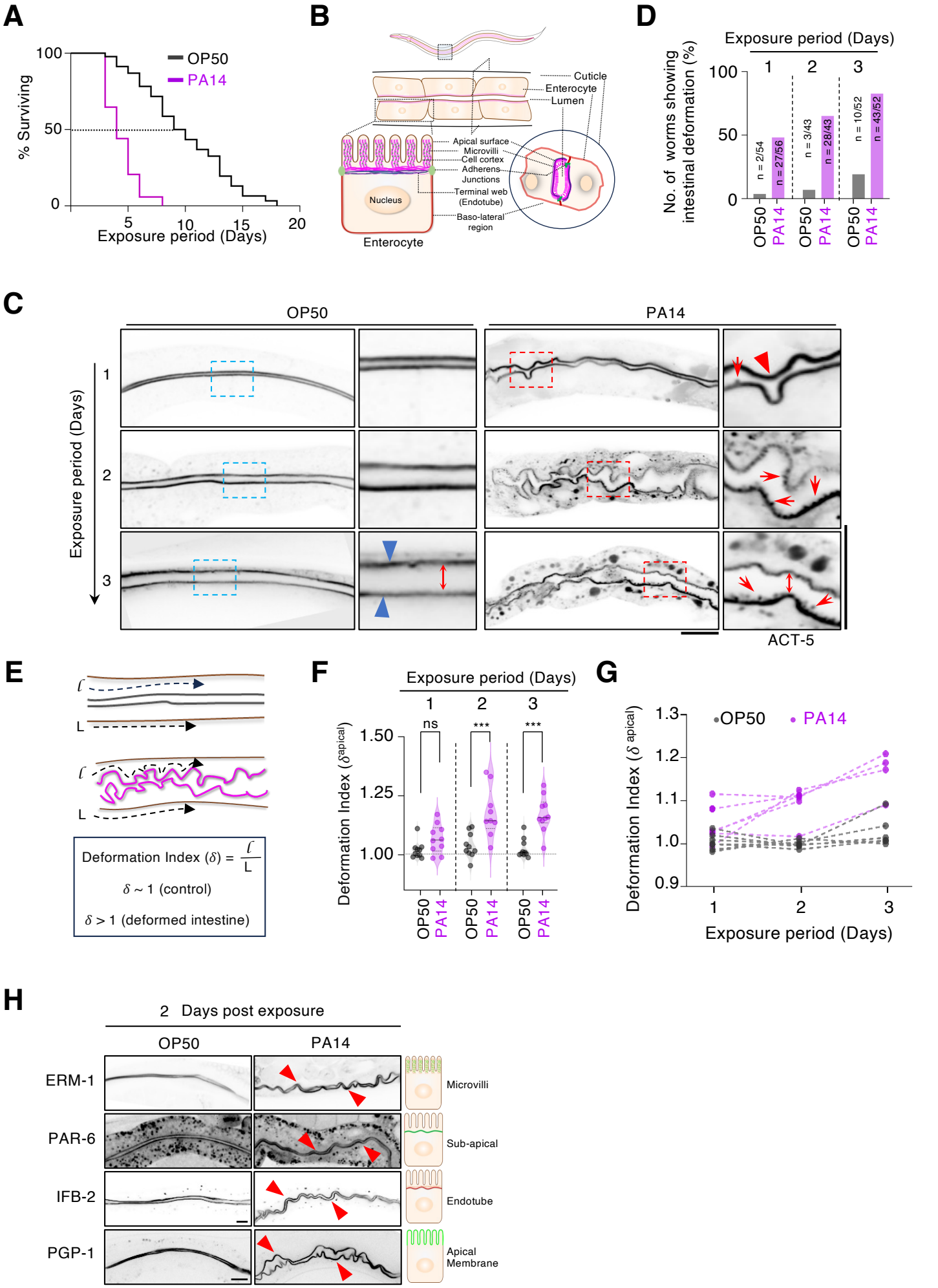

FIGURE LEGENDS

Figure 1: *P. aeruginosa* infection deforms the apical surface of intestinal epithelium in *C. elegans*

(A) Representative Kaplan-Meier survival plot of N2 worms infected with *P. aeruginosa* (PA14-magenta) or *E. coli* (OP50-black) at 25^0 C. (n = 100 worms, N=2)

(B) Schematic illustration of *C. elegans* intestinal epithelium depicting different regions of the enterocyte.

(C) Medial confocal sections of C. elegans intestines expressing mCherry::ACT-5 localized to apical surface. While lumen distension increases with age in animals exposed to with *P. aeruginosa* or *E. coli* (red double headed arrows), intestinal surface deformation is seen only upon exposure to with *P. aeruginosa* (red filled arrowheads), but not *E. coli* (blue ROI; blue filled arrowheads). with *P. aeruginosa* infection also led to actin vesicles budding of apical surface (Red ROI; red arrows).

(D) Bar graphs showing increased percentage of intestinal deformation with increase in the duration of exposure to with *P. aeruginosa*.

(E) Schematic showing the estimation of deformation index (δ^{apical}) of apical surface

(F) Representative violin plot showing quantification of deformation index of apical surface shown in Fig.1C. (N=3; n= 10 worms per treatment per set).

(G) Plot showing progressive deformation of apical surface of intestinal lumen from individual worms measured over 3 days following *P. aeruginosa* or *E. coli* exposure. (n=5)

(H) Medial confocal images of *C. elegans* expressing fluorescently labelled apical markers upon exposure to *P. aeruginosa* or *E. coli*. ERM-1::eGFP (apical regions containing microvilli), PAR-6::mNeonGreen (apical PAR polarity complex), IFB-2::wScarlet (intermediate filaments), PGP-1::GFP (apical plasma membrane).

Scale bar is 20 μm. P-values were calculated by Mann-Whitney U test. ****$p<0.0001$, ***$p<0.001$, and * $p<0.05$

Figure 2

Divyashree et. al (2025)

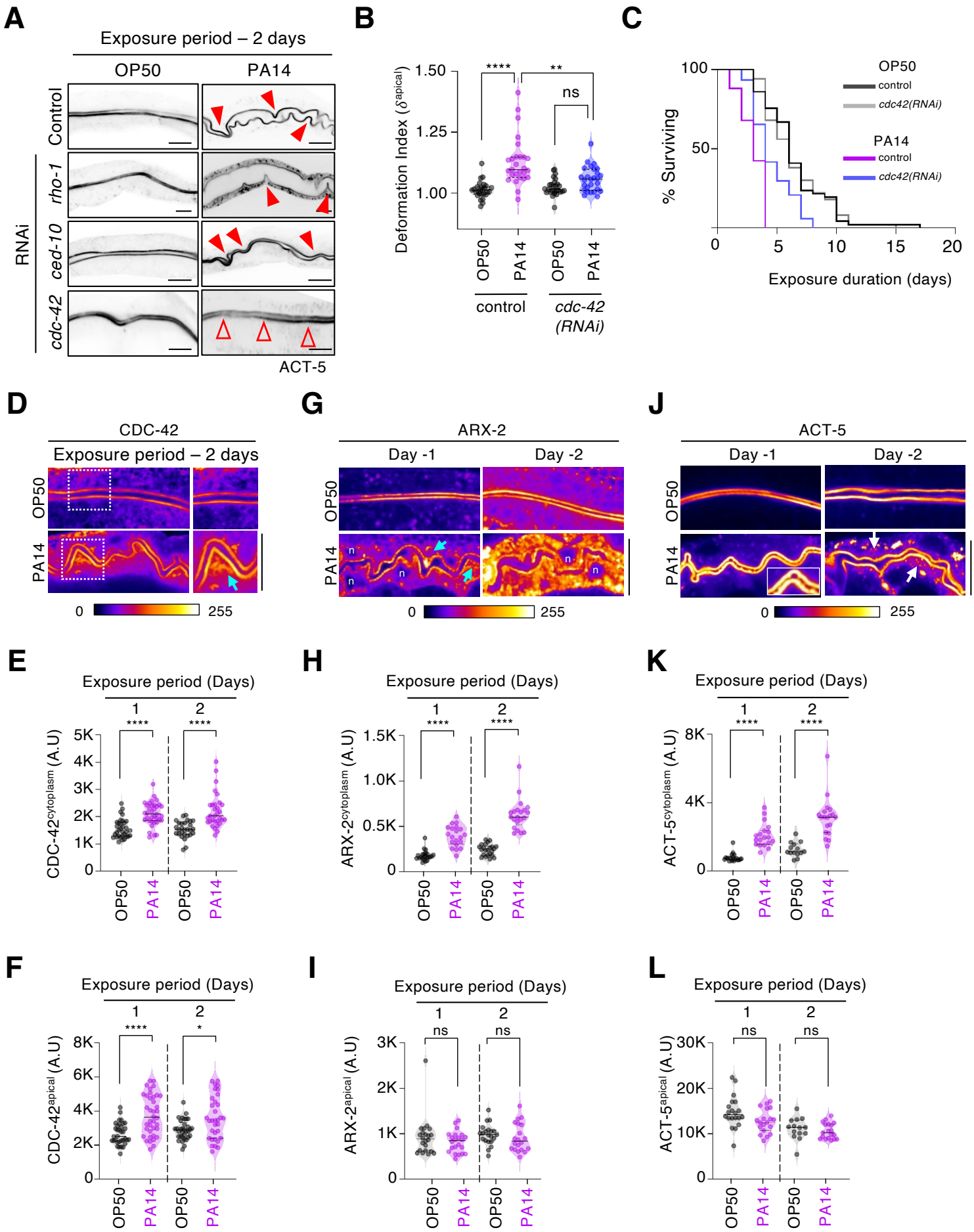

Figure 2: Exposure to *P. aeruginosa* results in cytoplasmic mis-localization of CDC-42, ARX-2 and ACT-5

(A) RNAi mediated depletion of *cdc-42*, but not *rho-1 or ced-10* rescues the *PA-14* induced intestinal deformation. Red filled arrowheads arrow heads show deformed regions of the lumen, while red open arrow heads denote the smooth intestinal lumen surface in *cdc-42(RNAi)* worms.

(B) Quantification showing reduced deformation index of intestines in *cdc-42(RNAi)* worms compared to L4440 (control) upon *P. aeruginosa* exposure. Measurements are plotted as violin plot indicating median and interquartile of each data set. (N = 3; n≥12 worms per condition and per replicate)

(C) Representative Kaplan-Meier survival plot of *cdc-42(RNAi)* or L4440 (control) worms subjected to *P. aeruginosa* or *E. coli* infection. CDC-42 depletion partially rescues *P. aeruginosa* induced shortening of lifespan ($TD50^{cdc42(RNAi)}$ = 8 days, $TD50^{control}$ = 4 days) (N=2; n= 50 worms per set and per condition)

(D, G and J) Medial cross-sections of intestinal lumen of *C. elegans* expressing (D) CDC-42::GFP, (G) ARX-2::TagRFP, and (J) mCherry::ACT-5 following exposure to *E. coli* or *P. aeruginosa*. Images shown are pseudo-colored to highlight changes in the intensity. Warm colors represent higher intensity and lower intensity by the dimmer colors. Cyan arrows indicate the cytoplasmic enrichment of these proteins in animals infected with *P. aeruginosa*. Where visible, nuclei of the intestinal cells are marked with letter 'n'. Scale bar -20 μm.

(E and F) Violin plots showing cytoplasmic (E) and apical (F) intensities of CDC-42::GFP upon *P. aeruginosa* or *E. coli* infection. Measurements are mean ±95% C.I. Each dot represents one animal and the data shown is the cumulation of three independent experiments (N=3; n=33).

(H and I) Violin plots indicating cytoplasmic (E) and apical (F) intensities of ARX-2::TagRFP upon *P. aeruginosa* or *E. coli* infection. Measurements are mean ±95% C.I. Each dot represents individual worm (N=2; n≥21)

(K and L) Violin plots of cytoplasmic (E) and apical (F) intensity measurements of mCherry::ACT-5 upon *P. aeruginosa* or *E. coli* infection. Measurements are mean ±95% C.I. Each dot represents individual worm (N=2; n≥14)

Scale bar is 20 μm. P-values were calculated by Mann-Whitney U test. ****p<0.0001, ***p <0.001, **p <0.01and * p <0.05.

Figure 3

Divyashree et. al (2025)

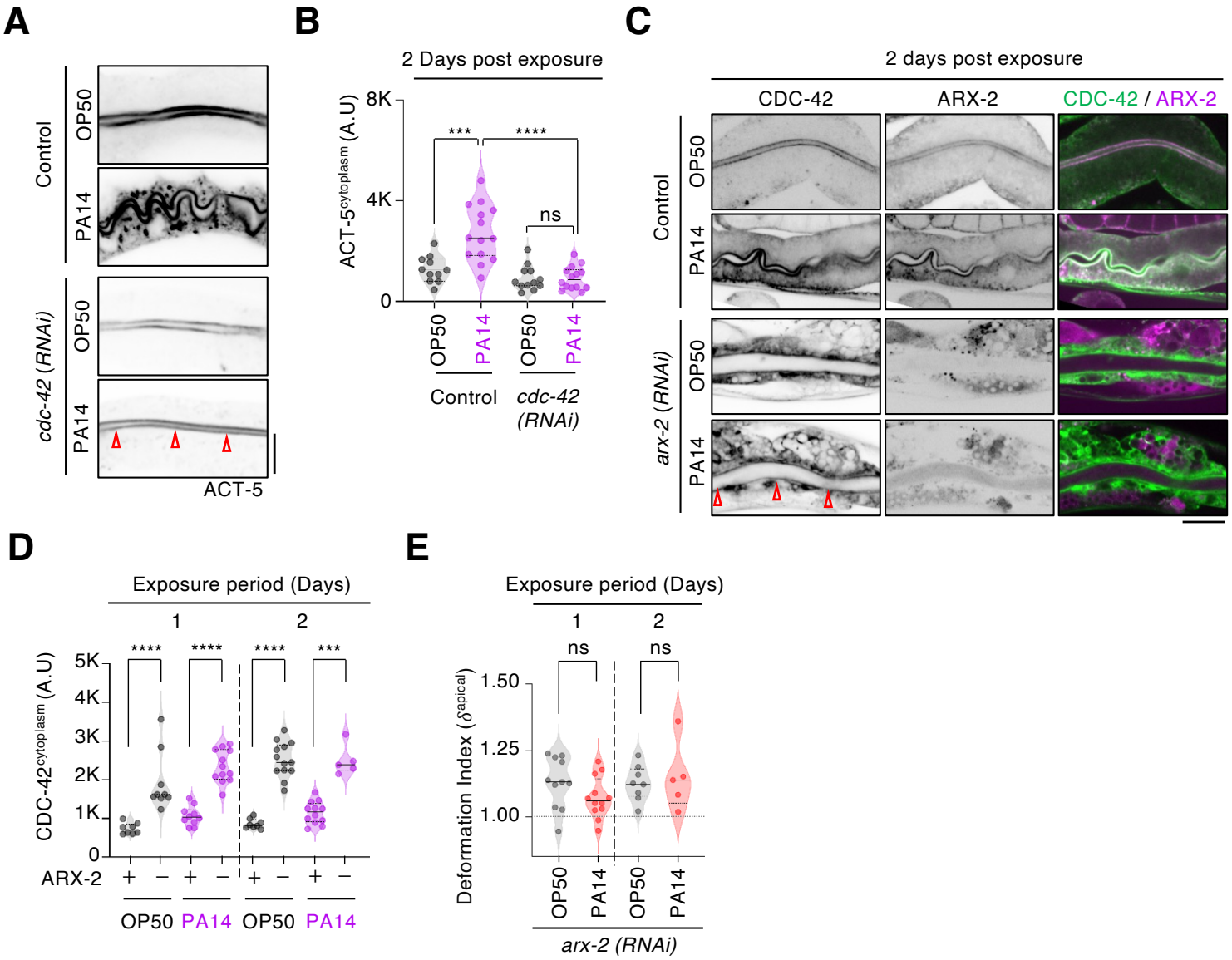

Figure 3: Inhibition of ARP-2/3 dependent actin polymerization prevents *P. aeruginosa* -induced apical surface deformation

(A) Intestinal lumen marked by mCherry::ACT-5 from control and *cdc-42(RNAi)* animals exposed to *P. aeruginosa* or *E. coli*. Red arrowheads indicate rescue of intestinal deformation in *cdc-42(RNAi)* animals.

(B) Cytoplasmic ACT-5 intensity quantified from intestinal epithelium of control and *cdc42(RNAi)* worms, day 2 post infection. Quantifications are mean ±95% C.I. (n ≤ 14).

(C) Confocal images of intestinal epithelium from control and *arx-2(RNAi)* animals co-expressing CDC-42::GFP and ARX-2::tagRFP, and subjected to *E. coli* and *P. aeruginosa* infection. All images are from 2- days post infection. Open red arrows indicate rescue of the intestinal deformation.

(D) Quantification of cytoplasmic CDC-42::GFP in control and *arx-2(RNAi)* animals following 2-day exposure to *P. aeruginosa* or *E. coli*. The violin plot shows the distribution of data with median and interquartile for each data set. p-values n≥8 for all the sets. expect n= 5 for PA14 *arx-2 (RNAi)*.

(E) Violin plot showing apical deformation index quantification for *arx-2(RNAi)* animals exposed to *E. coli* or *P. aeruginosa*. Plot shows the median and interquartile of each data set. (n ≤ 11).

(F) Medial plane image of intestinal lumen co-expressing PGP1::GFP and mCherry::ACT5 subjected to control (L4440) and *arx-2* RNAi followed by *E. coli* and *Pseudomonas* exposure. All the images are from one day post *E. coli* and *Pseudomonas* exposure.

(G) Medial plane image of intestinal lumen co-expressing CDC42::GFP and ARX2::TagRFP subjected to control (L4440, empty vector) and *act-5* RNAi followed by *E. coli* and *Pseudomonas* exposure. All the images are from one day post *E. coli* and *Pseudomonas* exposure. Open red arrow marks represent rescue of the intestinal deformation.

unless otherwise specified, Scale bar is 20 μm. P-values were calculated by Mann-Whitney U test. ****p<0.0001, ***p <0.001, and * p <0.05.

Figure 4

Divyashree et. al (2025)

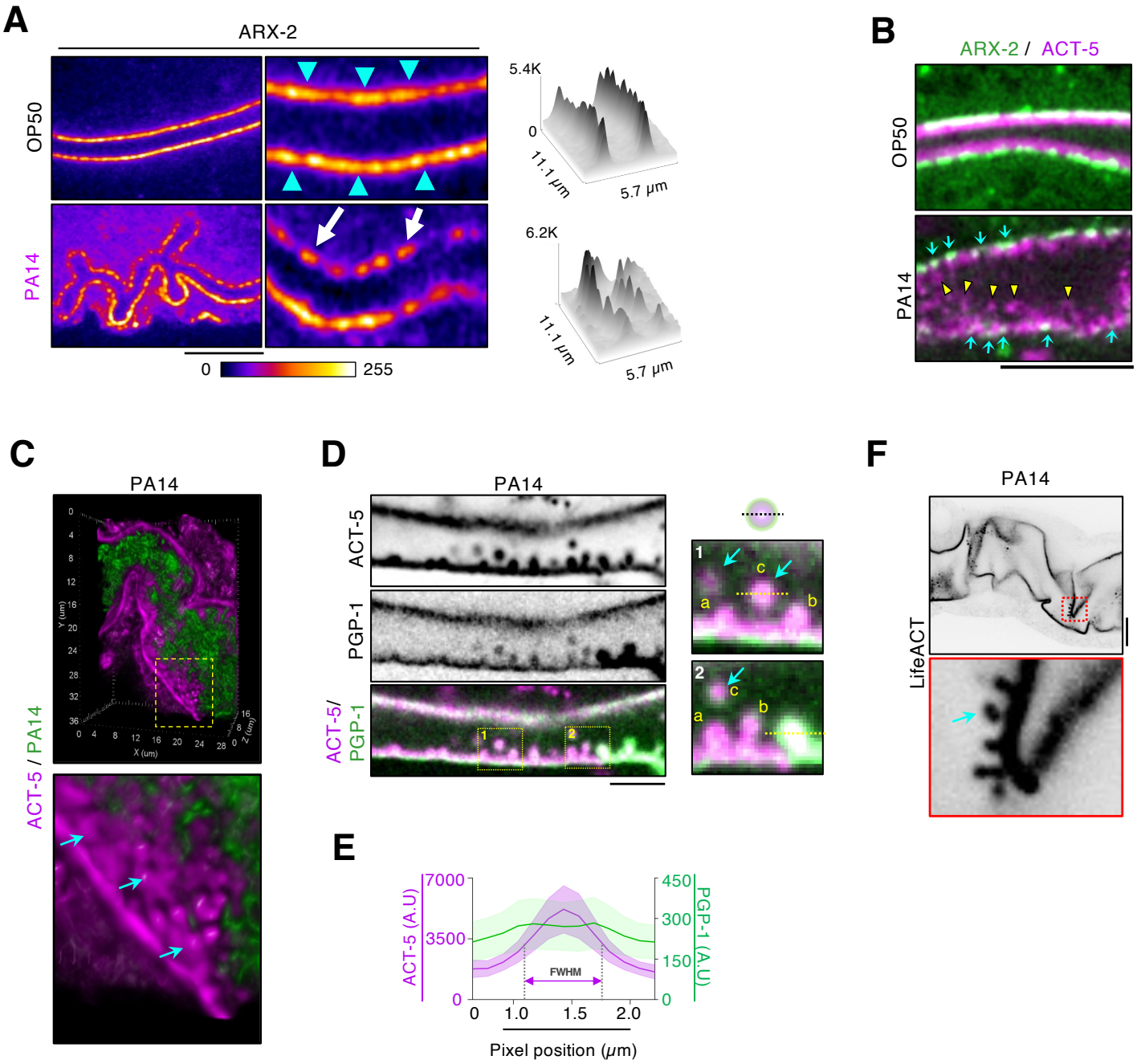

Figure 4: Fragmented ARP-2/3 disrupts actin assembly leading to extracellular vesicle release from apical surface

(A) Intensity visualization of medial confocal images of *C. elegans* intestines expressing ARX-2::TagRFP showing a fragmented distribution of ARX-2 (cyan arrows) on day-2 post *P. aeruginosa* exposure. ARX-2 shows a contiguous localization in worms exposed to *E. coli* (cyan arrowheads). Surface intensity of plots of enlarged ROIs highlights the fragmentation. Scale bar -10 μm.

(B) *C. elegans* co-expressing ARX-2::GFP and mCherry::ACT-5 showing actin structures (yellow arrowheads) permeating into the lumen from ARX-2-free regions (cyan arrows). Scale bar -10 μm.

(C) Lattice light sheet images acquired 2 days post exposure of PA14-GFP or OP50-GFP -fed *C. elegans* expressing intestinal mCherry::ACT5. Images were acquired in 13.3X objective and represented as maximum intensity projection in volume mode. Cyan arrows in enlarged ROI indicate the vesicles emerging from apical surface into the lumen.

(D) Membrane bound actin rich vesicles bud off from intestinal apical surface following 2-day *P. aeruginosa* exposure (cyan arrows in ROI). Enlarged ROI shows vesicles at various stages of budding – (a) initial bulging, (b) bud formation, and (c) released vesicle. An intensity linescan drawn across the extracellular vesicle indicates actin (magenta) surrounded by the apical plasma membrane marked by PGP-1::GFP (green). Scale bar - 5 μm.

(E) Line scan-intensity plot of mCherry::ACT5 and PGP1::GFP vesicles 2 days *P. aeruginosa* exposure. (n=20)

(F) LifeACT::mRuby localizes to F-actin in the apical vesicles (cyan arrow) of *C. elegans* intestines exposed to *Pseudomonas*. Scale bar - 10 μm.

P-values were calculated by Mann -Whitney U test. ****$p<0.0001$, ***$p<0.001$, and * $p<0.05$.

Figure 5

Divyashree et. al (2025)

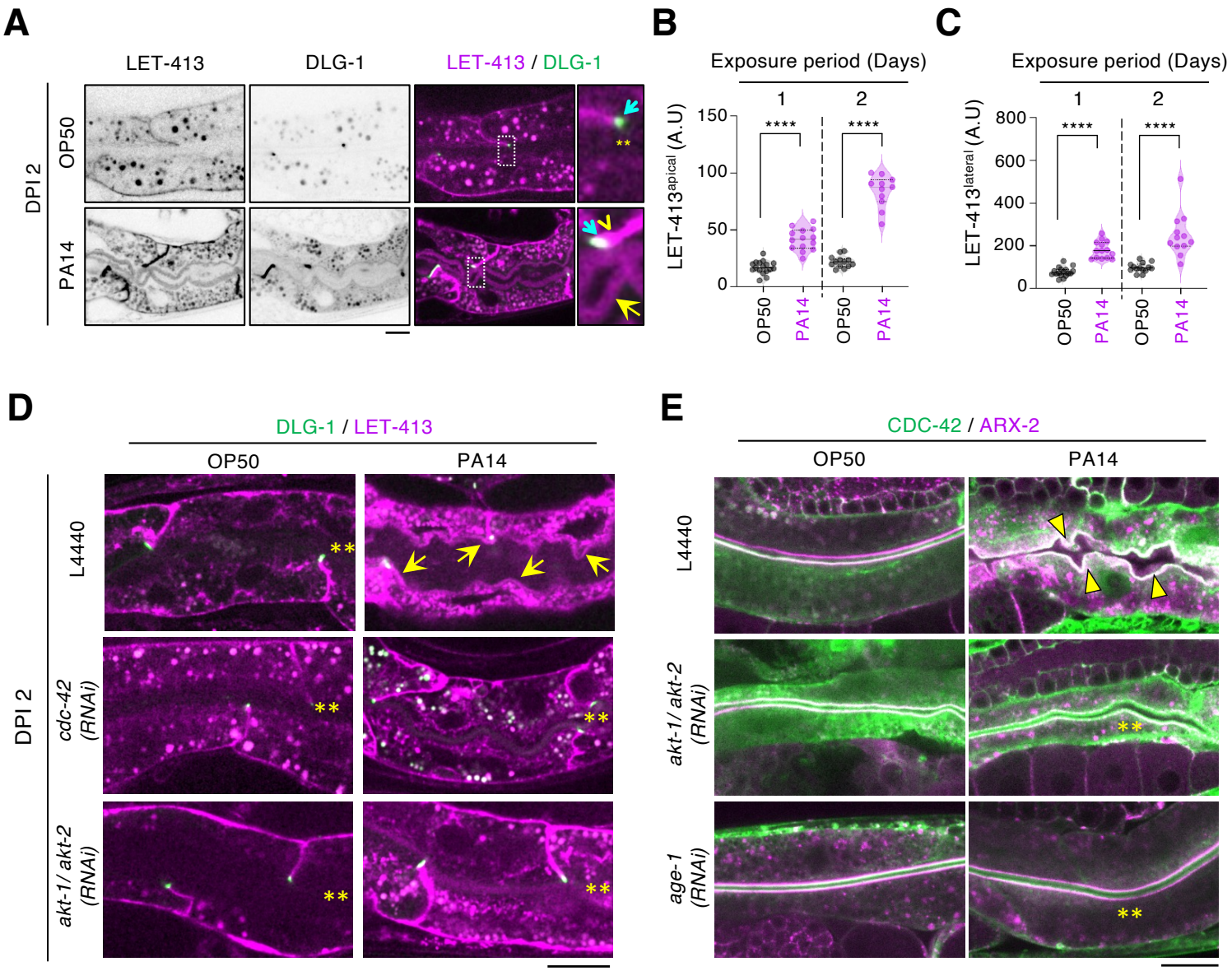

Figure 5 : *P. aeruginosa* induced polarity disruption is mediated via PI3K-AKT kinase pathway

(A) LET-413 shows enhanced accumulation in the apical (yellow arrow) and lateral (yellow arrowhead) surfaces *C. elegans* enterocytes upon *P. aeruginosa* infection. DLG-1 marks cell junctions (cyan arrows). Double asterisks shows absence of LET-413 at the apical surface in intestines of *C. elegans* exposed to *E. coli*.

(B and C) Quantification of (B) apical, and (C) cytoplasmic LET413 levels in enterocyte of worms following *E. coli* (OP50) or *P. aeruginosa* (PA14) infection. Each data point represents individual worm. Measurements are plotted as violin plot indicating median and interquartile of each data set. (n=12). p-value was calculated using Mann-Whitney U test. (n=12)

(A) Depletion of AKT-1 and AKT-2, or CDC-42 rescues *P. aeruginosa* induced loss of polarity. In contrast to control (L4440; yellow asterisks), apical recruitment of LET-413 in response to *P. aeruginosa* infection is absent in *akt-1/akt-2(RNAi)* and *cdc-42(RNAi)* (yellow asterisks).

(B) Disruption of PI3K-AKT pathway abrogates *P. aeruginosa* induced mis-localization of CDC-42, ARX-2 and actin. Medial confocal plane of intestinal lumen co-expressing CDC-42::GFP and ARX-2::TagRFP subjected to *akt-1/akt-2 and age-1* RNAi followed by *E. coli* and *Pseudomonas* exposure for two days. Closed yellow arrow indicate intestinal deformation. Yellow asterisks denote rescue of deformation.

Scale bar in 20 μm. P-values were calculated by Mann -Whitney U test. ****$p<0.0001$, ***$p<0.001$, and * $p<0.05$

Figure 6

Divyashree et. al (2025)

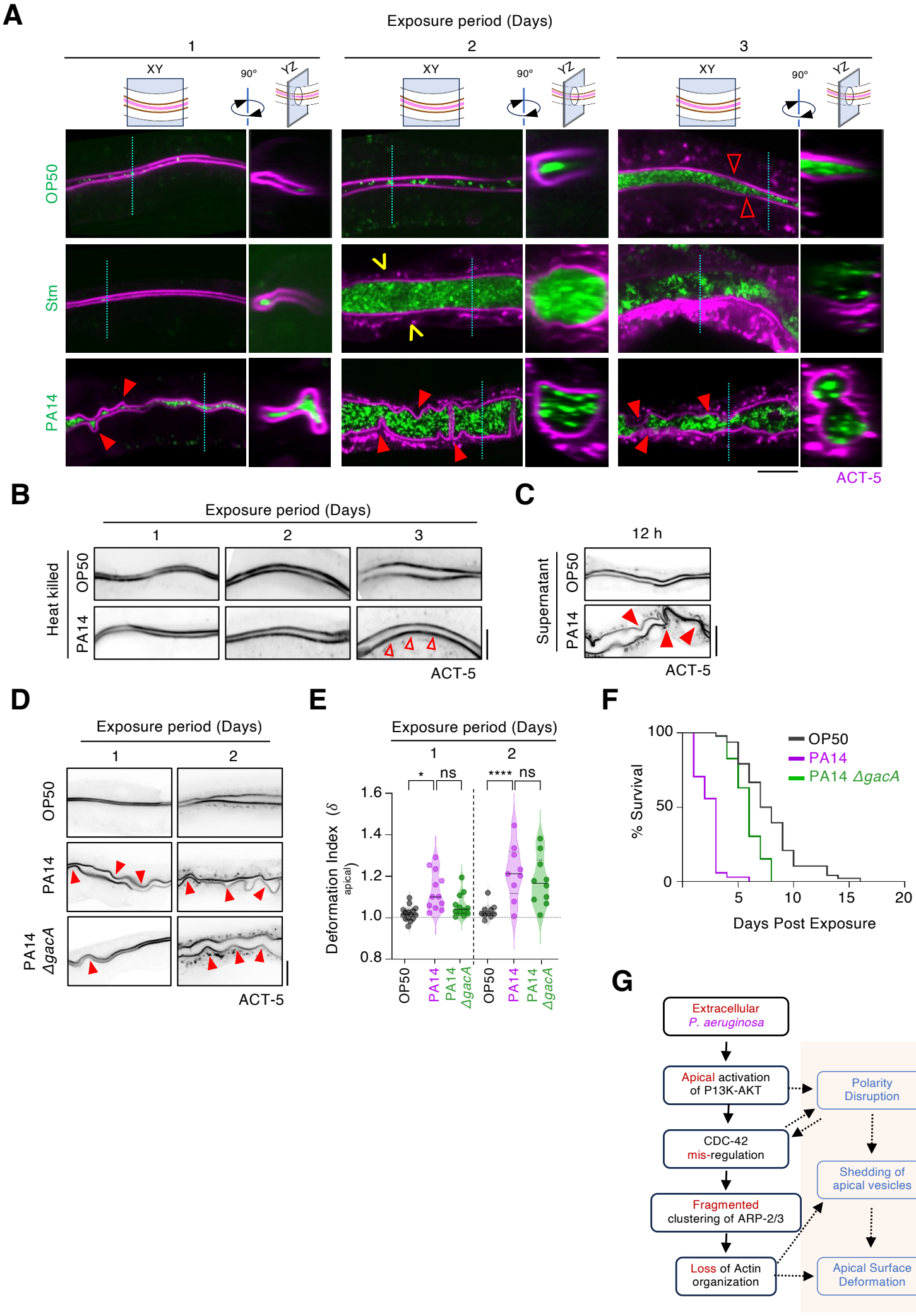

Figure 6: Extracellular *P. aeruginosa* can induce intestinal deformation in *C. elegans*

(A) Confocal medial images of intestinal epithelium from *C. elegans* expressing ACT-::mCherry and exposed to GFP expressing *E. coli* (top panel), *S. typhymurium* (middle panel) and *P. aeruginosa* (bottom panel) for 3-days post infection. Dashed lines indicate cross-sectional plane whose orthogonal view is presented adjacent to the image. Red hollow (*E. coli*) and yellow (*S. typhimurium)* arrowheads indicate intestinal distension (bloating), but smooth lumen surface. Red filled arrowheads indicate the deformation of the intestine in worms infected with *P. aeruginosa*. Scale bar - 20 μm.

(B) Medial confocal images of intestines from *C. elegans* expressing mCherry::ACT-5 animals grown on heat killed *E. coli* (top panel) and *P. aeruginosa* (bottom panel). Hollow red arrow indicates the absence of intestinal deformation upon exposure to heat killed *P. aeruginosa*. Scale bar- 20 μm.

(C) Medial confocal images of intestines from *C.* elegans expressing mCherry::ACT-5 exposed to *E. coli*(OP50) (top panel), *P. aeruginosa* (PA14) (middle panel) and *P. aeruginosa* (PA14ΔgacA) (bottom panel). Filled red arrows indicates intestinal deformation. Scale bar - 20 μm

(D) Quantification of deformation index (δ^{apical}) of the apical intestinal surface in C. elegans expressing intestinal mCherry::ACT-5 exposed to *E. coli*(OP50) ,*P. aeruginosa* (PA14) and *P. aeruginosa.* Each data point represents individual animal and measurements are plotted as violin plot indicating median and interquartile of each data set. (n =10)

(E) Kaplan- Meier survival plot of worms described in Fig. 6A upon exposure to *E. coli*(OP50) , *P. aeruginosa* (PA14) and *P. aeruginosa* . Worms were grown on *E. coli* till L4 stage and transferred on to the respective infection plates. (n = 50 worms, N=2)

(F) Schematic representation of the proposed mechanism for *P. aeruginosa* intestinal apical surface deformation in *C. elegans*

Scale bar in 20 μm. P-values were calculated by Mann -Whitney U test. ****$p<0.0001$, ***$p<0.001$, and * $p<0.05$